Title

A Ru265 analogue coordinated to cytotoxic pyrrolidine dithiocarbamate ligands for dual-function anticancer activity

Journal

Inorganic Chemistry Frontiers

ISSN

2052-1545

Authors

Zou, Haipei

Wilson, Justin J

Publication Date

2026

DOI

10.1039/d6qi01385f

A Ru265 analogue coordinated to cytotoxic pyrrolidine dithiocarbamate ligands for dual-function anticancer activity

Haipei Zou [a,b], Justin J. Wilson [a,b,*]

[a] Department of Chemistry and Biochemistry, University of California Santa Barbara, Santa Barbara, California 93106, United States

[b] Department of Chemistry and Chemical Biology, Cornell University Ithaca, New York 14853, United States

* Corresponding author: justinjwilson@ucsb.edu

Keywords:
metals in medicine, mitochondrial calcium uniporter, ruthenium, dithiocarbamate, anticancer

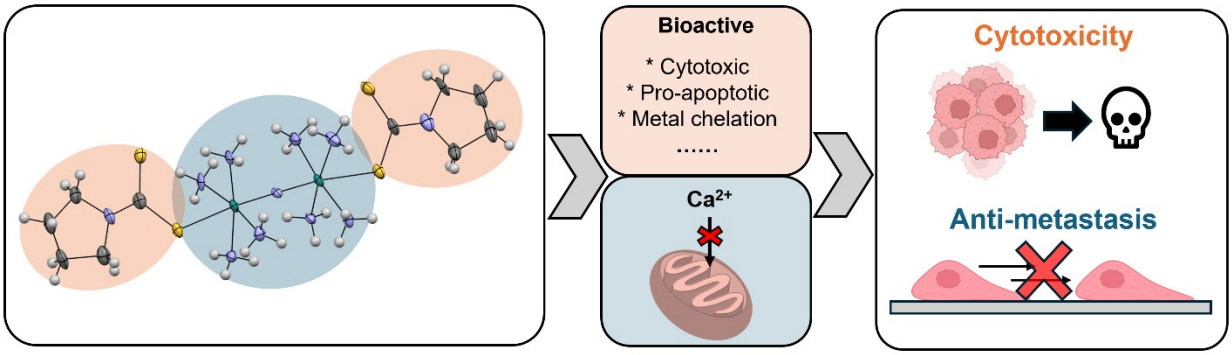

Abstract

Triple negative breast cancer (TNBC) is an aggressive breast cancer subtype with high metastatic potential and limited treatment options. Herein, we developed a dual-function anticancer agent **RuSPDTC** ($[Ru_2(\mu\text{-}N)(NH_3)_8(S_2CN(CH_2)_4]^{3+}$) by attaching the cytotoxic pyrrolidine dithiocarbamate (PDTC) ligand to the mitochondrial calcium uniporter (MCU) inhibitor Ru265 ($[Ru_2(\mu\text{-}N)(NH_3)_8Cl_2]^{3+}$). **RuSPDTC** combines the anti-metastatic activity of MCU inhibition with PDTC-mediated cytotoxicity within a single molecular platform. **RuSPDTC** was synthesized and characterized by multinuclear NMR spectroscopy, HR-ESI-MS, FTIR spectroscopy, UV-vis spectroscopy, and single-crystal X-ray diffraction. The ^{13}C resonance of the CS_2 group showed a upfield shift of the coordinated PDTC ligands, and HR-ESI-MS revealed an *m/z* of $[M–CF_3SO_3]^+$ at 943.9475 Da. These data confirmed the coordination of PDTC to the Ru265 scaffold. The crystal structure of **RuSPDTC** showed that PDTC coordinates to Ru through S at the axial positions, representing the first Ru265 analogue featuring a S-donor ligand. UV-vis kinetic studies demonstrated its aquation under physiological conditions with a half-life of 2.4 h, leading to the quantitative release of bioactive Ru265′ ($[Ru_2(\mu\text{-}N)(NH_3)_8(OH_2)_2]^{5+}$) and two equivalents of PDTC. Within MDA-MB-231 TNBC cells, **RuSPDTC** exhibited potent Cu^{2+}-dependent cytotoxicity with an IC_{50} value of 0.07 μM in the presence of 10 μM Cu^{2+}, a value that is two orders of magnitude smaller than that in the absence of Cu^{2+}. Importantly, **RuSPDTC** retained potent MCU-inhibitory activity with an IC_{50} value of 4.23 nM and effectively suppressed cancer cell invasion and migration. Overall, this work establishes a proof-of-concept study for developing dual-function Ru265-based therapeutics integrating cytotoxic and anti-metastatic activities into a single scaffold through incorporation of bioactive ligands.

Introduction

The most recent Cancer Statistics Report from the American Cancer Society reveals that breast cancer is the most common cancer among women in the US and has become the leading cause of cancer-related death among women under 50 years old.[1] Given the significant threat of breast cancer posed to human health, many efforts have been focused on studying its mechanism of pathogenesis, as well as the development of therapeutic strategies. There exist different subtypes of breast cancer based on different expression levels of hormone receptors, among which triple negative breast cancer (TNBC) is the most aggressive and difficult to treat. This subtype lacks the expression of the drug-targetable estrogen receptor, progesterone receptor, and human epidermal growth factor receptor 2, which are ubiquitous in other subtypes.[2] Although breast cancer starts as a local disease, cancer cells metastasize and spread through blood and lymphatic vessels to distant organs in the body, making treatment more challenging.[3] Standard therapeutic strategies for breast cancer consist of local removal of the tumor through surgery or radiation, followed by systematic treatment to prevent reoccurrence and to target metastatic lesions.[4,5] Because TNBC lacks the three targetable hormone receptors, broad spectrum cytotoxic chemotherapy still remains the main treatment strategy.[5] Consequently, the prognosis of TNBC patients substantially worse than

patients with other subtypes.[5–8] As such, there is an urgent need to develop new and effective drugs to prolong patient lives.

The mitochondrial calcium uniporter (MCU), which is located in the inner mitochondrial membrane, is the main transporter that mediates uptake of calcium ions (Ca^{2+}) by the mitochondria and is therefore critical in the regulation of mitochondrial function.[9,10] Acute mitochondrial Ca^{2+} ($_mCa^{2+}$) overload triggers the opening of the mitochondrial permeability transition pore (mPTP), leading to the formation of reactive oxygen species (ROS), release of cytochrome c, and apoptosis.[11,12] The promotion of ROS levels by $_mCa^{2+}$ overload can induce pro-tumorigenic redox signaling pathways that may enhance cancer cell survival.[13–15] Furthermore, high $_mCa^{2+}$ levels have been correlated to metastasis. Prior studies have demonstrated that inhibition, knockdown, or knockout of the MCU in TNBC cell lines can significantly reduce metastasis in both in vitro and in vivo models.[16–20] Given the role that the MCU plays in tumorigenesis and metastasis, the MCU is a promising target for breast cancer.[21]

Our lab has developed an effective inorganic MCU inhibitor Ru265 ($[Ru_2(\mu\text{-}N)(NH_3)_8Cl_2]^{3+}$) that is a close analogue of the previously reported Ru-based MCU inhibitor Ru360 ($[Ru_2(\mu\text{-}O)(NH_3)_8(O_2CH)_2]^{3+}$). Compared to Ru360, Ru265 offers the advantage of being significantly more stable than Ru360,[22,23] and this property has enabled more extensive use of Ru265 in different biological models. As part of its mechanism of action, Ru265 aquates rapidly in physiological conditions ($t_{1/2}$ = 2.3 min) to form Ru265′ ($[Ru_2(\mu\text{-}N)(NH_3)_8(OH_2)_2]^{5+}$), and this species is considered to be the active MCU inhibitor.[22,24,25] This compound not only exhibits high MCU inhibition potency with a nanomolar IC_{50}, but also offers a versatile scaffold for prodrug development. Through substitution of axial chloride with other ligands, we are able to introduce new functionalities that can prolong the prodrug activation kinetics,[26] improve cellular uptake,[27–29] exhibit fluorescence,[30] and undergo pH-dependent activation.[29] Based on the efficacy of Ru265 and its analogues as MCU inhibitors and the fact that the MCU regulates cancer progression, we believe that Ru265 derivatives could be optimized to become promising therapeutic agents for TNBC. Because these complexes are not cytotoxic, however, the MCU-inhibitory properties of these compounds are only expected to result in anti-metastatic activity, limiting their versatility for managing this disease. An alternative approach to increase their therapeutic viability is to use cytotoxic axial ligands that could potentiate cell death pathways. This strategy provides a dual-pronged approach, where the Ru265′ core structure could inhibit the MCU and prevent metastasis, while the cytotoxic axial ligands could actively kill the cancer cells. As a potential cytotoxic axial ligand, pyrrolidine dithiocarbamate (PDTC) was considered, based in part on the efficacy of dithiocarbamates as ligands for metal centers. This ligand has long been investigated as an anticancer and anti-inflammatory agent since the discovery of its ability to inhibit the nuclear factor NF-κB pathway.[31–33] PDTC can also act as an effective antioxidant through ROS scavenging and the induction of glutathione synthesis to reduce oxidative stress.[34,35] Through the chelation of bioactive metal ions like copper(II) (Cu^{2+}) and zinc(II) (Zn^{2+}), PDTC can increase the intracellular level of these metals and trigger metal-mediated cytotoxicity.[36–39] On the basis of these properties and in recognition of the ability of this compound to act as a ligand, researchers have investigated

the potential of metal-PDTC complexes for therapeutic applications, with a particular emphasis on complexes of ruthenium (Ru).[40–43] Based on these prior studies, PDTC complexes of Ru265 are expected to be promising anticancer agents for TNBC.

To investigate this hypothesis, here we report a Ru265-based prodrug containing two PDTC axial ligands, named **RuSPDTC**. This compound is designed to be a dual-function anticancer agent, with the Ru265 core acting to reduce metastasis through MCU inhibition and the PDTC ligand inducing cytotoxicity. Both the physical and biological properties of this compound were investigated, demonstrating its potential as an aquation-activated prodrug for TNBC.

Results and discussion

Synthesis and characterization

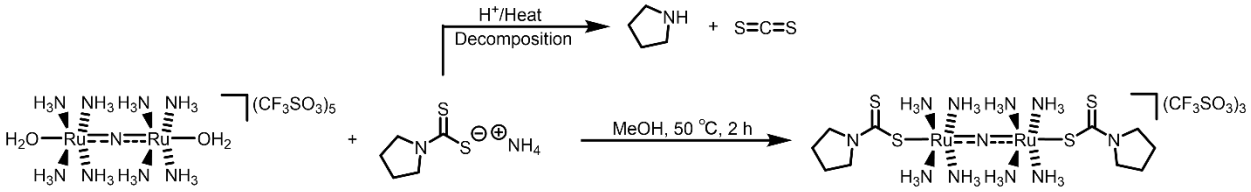

Scheme 1 Synthetic scheme for **RuSPDTC**.

RuSPDTC was synthesized following similar approaches used to make carboxylate- and phosphinate-capped analogues.[26–30] This synthesis required the treatment of Ru265′ with two equivalents of NH_4PDTC in methanol at 50 °C. Due to the instability of the PDTC ligand, which is a consequence of its tendency to form carbon disulfide and pyrrolidine at elevated temperatures and acidic pH values,[44,45] the reaction of this ligand with Ru265′ was only allowed to proceed for 2 h to minimize the formation of byproducts resulting from ligand decomposition. The crude product was purified by recrystallization twice through diffusion of diethyl ether vapor into a methanol solution of the compound at room temperature. **RuSPDTC** was characterized by multinuclear NMR spectroscopy, HR-ESI-MS, FTIR spectroscopy, UV-vis spectroscopy, and X-ray crystallography. The ^{1}H NMR spectrum (Fig. S1, SI) of **RuSPDTC** shows the ^{1}H resonance of the equatorial NH_3 ligands at $\delta = 4.12$ ppm. This chemical shift is more downfield shifted compared to Ru265′ and previously reported Ru265 analogues with axial oxygen donor ligands, which have chemical shifts for the NH_3 group that range between 3.89–4.08 ppm. This chemical shift, however, is more similar to that of the chloride-capped Ru265 ($\delta = 4.15$ ppm). The trend of changes in chemical shift upon coordination to different donor atoms is consistent with previously reported ^{15}N-labeled Ru265 ([^{15}N]Ru265), where [^{1}H,^{15}N] HSQC NMR spectroscopy revealed coordination of Ru to the thiol group on cysteine under physiological conditions with a ^{1}H resonance at 3.96 ppm, whereas Cl^--capped [^{15}N]Ru265 and H_2O-capped [^{15}N]Ru265′ showed ^{1}H resonances at 4.03 ppm and 3.73 ppm, respectively.[46] These results indicate that sulfur and chloride donors, with similar electronegativities, induce smaller shielding effects on protons of the equatorial NH_3 than the oxygen donors. The ^{1}H resonances of the PDTC ligands exhibits a downfield shift by ~0.1 ppm upon coordination (Fig. S1, SI), whereas the ^{13}C resonance of the RN*C*S_2^- carbon shows a significant upfield shift from 209 ppm to 198 ppm (Fig. S2, SI). In previously reported

ruthenium(II) dithiocarbamate (DTC) compounds, where DTC attains a bidentate coordination mode, the ^{13}C resonance of the $RNCS_2^-$ carbon exhibits a downfield shift instead.[47,48] The different changes in chemical shifts can be explained by considering the resonance forms of DTC (Scheme 2). For bidentate symmetric coordination modes, resonance structure (c) is the major contributor.[49] This resonance form signifies a high degree of polarity in the C–N bond, as discerned from the positive formal charge on the nitrogen, that withdraws electron density from the carbon center, leading to its deshielding. However, when the DTC coordinates as a monodentate ligand, the equivalent resonance structures (a) and (b) (Scheme 2) are most important, reflecting less polarization of the C–N bond and consequently a more electron-rich, shielded ^{13}C nucleus that leads to an upfield shift in its resonance.[50] For related gold(I) complexes containing monodentate DTC ligands, similar upfield shifts in the $RNCS_2^-$ carbon resonance are observed.[51,52] Within the ^{19}F NMR spectrum (Fig. S3, SI), **RuSPDTC** shows a single peak at –77.74 ppm, which is attributed to the outer-sphere triflate counterions. The HR-ESI-MS of **RuSPDTC** reveals a feature at *m/z* of 943.9475 Da. This peak and its resulting isotope distribution pattern correspond to a molecular ion in which **RuSPDTC** is ionized as a +1 cation via the loss of a single outer-sphere triflate anion (Fig. S4, SI). In addition to this parent molecular ion peak, a series of species between 860–927 Da were also apparent. These peaks differed by 17 *m/z*, reflecting fragmentation of the parent ion through loss of equatorial NH_3 ligands (Fig. S4, SI). The FTIR spectrum (Fig. S5, SI) of **RuSPDTC** shows diagnostic N–H stretching and bending modes of the NH_3 ligands at 3320 and 1625 cm^{-1}, respectively, as well as the C–N stretching mode of the PDTC ligands at 1421 cm^{-1}. The C–S stretching modes appear at 914 and 941 cm^{-1}, and the magnitude of the energy difference between these modes is consistent with the monodentate coordination of the DTC ligand within Ru complexes.[53] Although the asymmetric Ru–N–Ru stretching mode is expected around 1000–1100 cm^{-1}, this feature is challenging to conclusively assign because of the presence of other overlapping modes, like the symmetric SO_3 stretching mode that arises from the triflate counterion.[54] The UV-vis spectrum (Fig. S6, SI) of **RuSPDTC** shows maximum absorbance values at 253 nm (68000 ± 1500 $M^{-1}cm^{-1}$) and 324 nm (16450 ± 70 $M^{-1}cm^{-1}$) with absorbance values from weaker transitions trailing into the visible. To probe these transitions in more detail, time-dependent density functional theory (TD-DFT) calculations were employed. These TD-DFT calculations indicate that the absorbance at 324 nm is best assigned as a ligand-to-metal charge transfer (LMCT), reflecting an electronic transition between occupied S-based orbitals on the PDTC ligand to the empty Ru–N–Ru π* orbital. Collectively, these characterization data confirm the formation of **RuSPDTC**, marking this compound as the first example of a Ru265 prodrug that contains axial S-donor ligands.

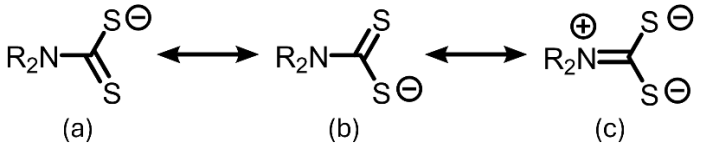

Scheme 2 Resonance structures of dithiocarbamate.

X-ray crystallography

Singe crystals of **RuSPDTC** suitable for X-ray diffraction were obtained from slow diffusion of cyclohexane vapor into a tetrahydrofuran solution of this compound (10 mg/mL) at 4 °C. The crystal structure of **RuSPDTC** is shown in Fig. 1, and relevant data collection parameters and interatomic distances and angles are collected in Tables S1–S2, SI. This structure confirms that the PDTC ligands bind to the Ru centers in a monodentate fashion with supporting hydrogen-bonding interactions apparent between the non-coordinating S atom of the PDTC ligand and the equatorial NH_3 ligands. The Ru–N–Ru backbone is nearly linear with an interatomic angle of 178.0(6)°. The four equatorial NH_3 ligands on the adjacent Ru centers are close to an eclipsed arrangement, with a dihedral angle between neighboring Ru(1)–N and Ru(2)–N bonds around 18°. In previously reported crystal structures of Ru265 and its analogues, both eclipsed and staggered arrangements have been observed,[24,26–30] reflecting small energy differences between these conformations. The interatomic distance between the Ru centers and the bridging N is 1.767(9) and 1.759(9) Å. These values are not appreciably different from previously reported Ru265 derivatives.[24,26–30] The interatomic distances between the Ru centers and the coordinating axial S atoms are 2.511(3) and 2.512(3) Å. These distances are significantly longer than other axial ligand distances within this compound class like Ru265 (Ru–Cl = 2.384 Å) and analogues with O donors (Ru–O = 2.076–2.119 Å).[24,26–30] The longer axial interatomic distances found within **RuSPDTC** can be readily explained by the larger atomic radius of S compared to Cl and O. In previously reported Ru(II)[42] and Ru(III)[41] compounds coordinated with PDTC in a bidentate manner, the interatomic Ru–S distances range between 2.375–2.454 Å. Only few Ru complexes with monodentate DTC ligands have been reported and investigated.[55–57] The only crystal structure we found for monodentate Ru-DTC was nitrosylruthenium tris(*N,N*-diethyldithiocarbamate) (*trans*-[Ru(NO)(κ^1-S_2CNEt_2)(κ^2-$S_2CNEt_2)_2$]) reported in 1966, revealing a Ru–S interatomic distance between Ru and monodentate DTC to be 2.398 Å.[55] The longer Ru–S distances within **RuSPDTC** are attributed to both the monodentate coordination mode as well as the trans influence of the bridging N^{3-} ligand. The C–S distances within the PDTC ligands are appreciably different. For the S directly coordinated to the Ru center, the C–S distances are longer by up to 0.06 Å compared to the C–S distances for the non-interacting S atoms. For Ru complexes with bidentate PDTC ligands, the C–S distances are not appreciably different from each other ($\Delta d < 0.02$ Å),[41,42] consistent with the predominance of resonance form (c) (Scheme 2) within this coordination mode. To our knowledge, **RuSPDTC** is the second reported crystal structure of Ru complex coordinated with DTC ligands in a monodentate manner.

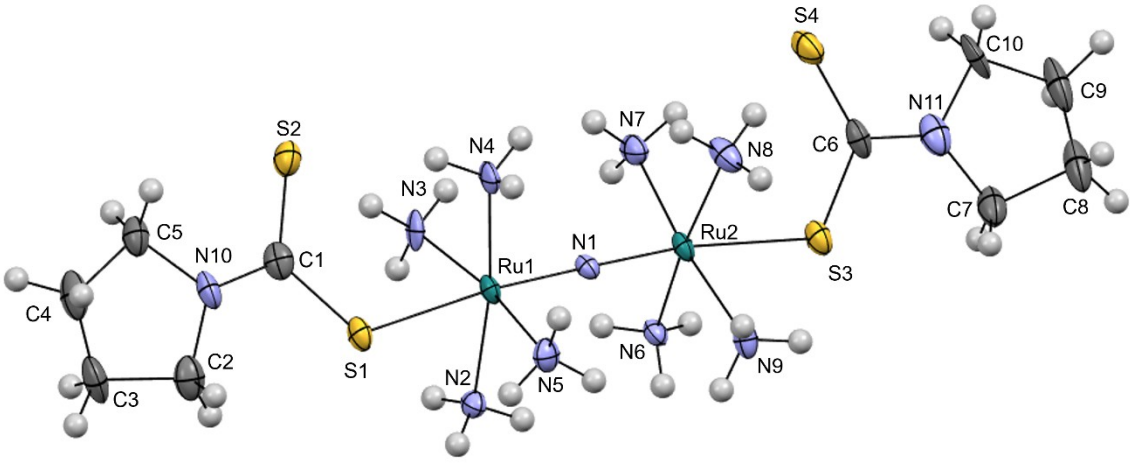

Fig. 1 Crystal structure of **RuSPDTC**. Thermal ellipsoids are shown at the 50% probability level. Solvent and counterion molecules are omitted for clarity. Atom colors: teal = Ru, gray = C, blue = N, yellow = S, white = H.

Aquation kinetics of RuSPDTC

RuSPDTC is designed to exhibit dual-function activity originating from both the Ru265′ core and the released PDTC ligands. For this dual-activity to be realized, **RuSPDTC** must undergo aquation in physiological conditions on a biologically relevant timescale. The absorbance at 324 nm, which arises from an LMCT excited state transition, provides a convenient spectroscopic signature for monitoring the dissociation of the PDTC ligands. Upon incubation of **RuSPDTC** in pH 7.4 MOPS buffer at 37 °C, this absorbance band decreased in a time-dependent manner, consistent with the aquation of the PDTC ligands (Fig. 2). The decay of this 324 nm absorbance band could be fit to a monoexponential function, consistent with a pseudo first order process. Although the aquation process should exhibit more complex kinetics, as a two-step A → B → C process,[26,46] like other Ru265 prodrugs the aquation of the first axial ligand is significantly slower than the second axial ligand dissociation, allowing a simple pseudo first order kinetic process to be used to assess the overall complex stability.[27–30] This data fitting process revealed a half-life of 2.4 ± 0.1 h under these physiologically relevant conditions (Fig. 2). This half-life is longer than that for a related phosphinate-capped analogue ($t_{1/2}$ = 1.7 ± 0.2 h)[29] and shorter than that for the carboxylate-capped analogues ($t_{1/2}$ = 3.3–9.9 h).[26–28,30] The overall trend in aquation half-life values within this compound class appears to follow the basicity of the axial ligands. More basic ligands, reflected by higher conjugate acid p*K*a values, give rise to longer aquation half-lives (Table 1). This result can be rationalized by stronger electron-donating properties of more basic ligands, which leads to more inert axial Ru–ligand bonds. Also apparent in Fig. 2 is the complete bleaching of the 324 nm absorbance band after 17 h, indicating that the PDTC ligands fully dissociate and that an equilibrium with partial ligand association is not apparent, as was previously observed for phosphonate-capped analogues.[29] Previous extended X-ray absorption fine structure (EXAFS) studies of Ru265′ reveal it to be stable under physiological conditions, even in the presence of

biological reductants and in whole human blood.[23] Likewise, the ligand PDTC also stays intact, as shown by the analysis of its UV-vis spectrum under identical conditions (Fig. S7, SI).[44] Therefore, these studies show that **RuSPDTC** undergoes aquation at a biologically relevant timescale to release the bioactive Ru265′ core and free PDTC ligands, laying a solid foundation for the use of this compound as a dual-function therapeutic agent.

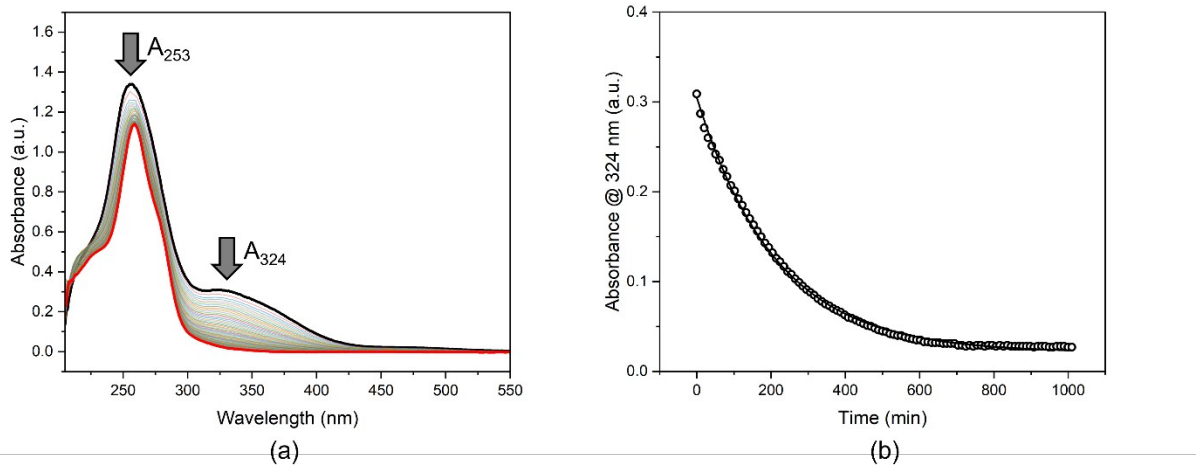

Fig. 2 UV-vis kinetic study for **RuSPDTC**. (a) Representative UV–vis spectra of **RuSPDTC** collected every 10.2 min during aquation in MOPS buffer (pH = 7.4) at 37 °C. (b) The absorbance at 324 nm traced over time to calculate the half-life of aquation.

Table 1 p*K*a of free ligands (conjugate acid forms) and aquation half-lives ($t_{1/2}$) of corresponding Ru265 analogues at physiological condition (37 °C, pH = 7.4)

	HCO_2H	$(CH_2)_4NCS_2H$	Ph_2PO_2H
p*K*a	3.8	3.2	2.3
$t_{1/2}$ (h) of corresponding Ru265 analogue	3.3 ± 0.1[a]	2.4 ± 0.1	1.7 ± 0.2[b]

[a] Ref. 26. b Ref. 29.

Cu^{2+}-induced aquation of RuSPDTC

PDTC is an effective chelator for Cu^{2+} that forms the square planar $Cu(PDTC)_2$ complex.[58] Given that Cu is an essential element in biology, we investigated the Cu^{2+}-responsive activation of **RuSPDTC**. In this experiment, **RuSPDTC** was mixed with $CuSO_4$ at varying concentrations (millimolar regime) in dimethylformamide (DMF) under ambient conditions. Upon mixing, an immediate color change was observed, indicating a rapid reaction between **RuSPDTC** and $CuSO_4$ (Fig. S8, SI). Furthermore, the color change is identical to that observed after the reaction between PDTC and $CuSO_4$ (Fig. S8, SI). UV-vis spectroscopic analysis of the reaction mixtures revealed a decrease in the characteristic absorbance bands of **RuSPDTC** at 324 nm dependent on Cu^{2+} concentrations, accompanied by the emergence of a new absorbance band at 434 nm, consistent

with the formation of $Cu(PDTC)_2$ (Fig. 3). These observations suggest that Cu^{2+} competes for the coordination with PDTC, promoting cleavage of the Ru–S bond and inducing aquation of **RuSPDTC** (Scheme 3). However, compared with the reaction between $CuSO_4$ and PDTC, **RuSPDTC** yields less $Cu(PDTC)_2$ formation, as evidenced by the lower absorbance at 434 nm. This observation indicates that although Cu^{2+}-induced aquation of **RuSPDTC** occurs instantaneously, the reaction is not complete within the short reaction time. The rapid kinetics of this process align with the strong affinity of PDTC towards Cu^{2+} and provide direct evidence that **RuSPDTC** can undergo Cu^{2+}-mediated activation under biologically relevant conditions.

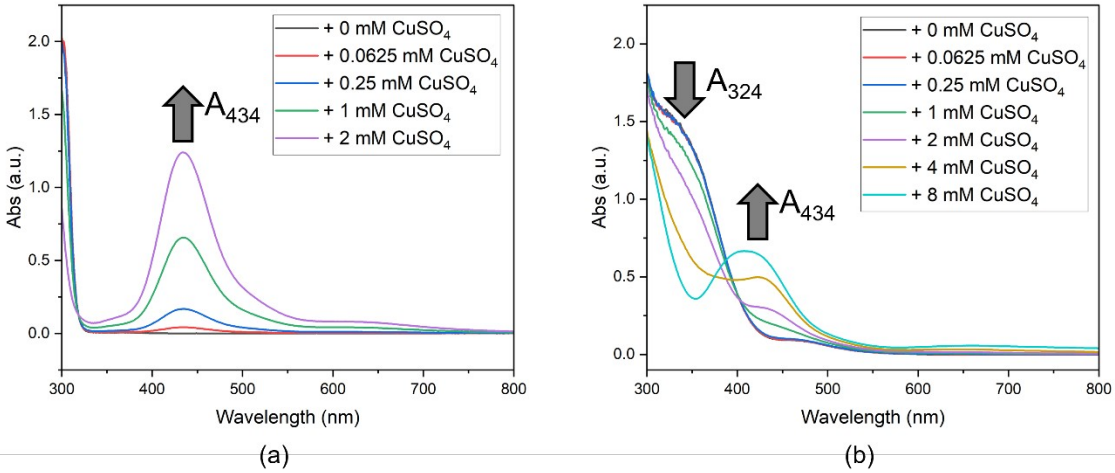

Fig. 3 UV-vis spectra of reaction between (a) 4 mM PDTC or (b) 2 mM **RuSPDTC** with $CuSO_4$ at varying concentrations in DMF at room temperature.

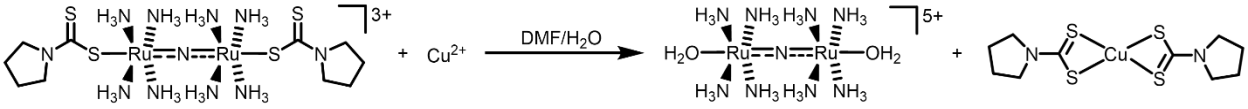

Scheme 3. Reaction scheme proposed for Cu^{2+}-induced aquation of **RuSPDTC**.

Cellular uptake and Cu^{2+}-dependent cytotoxicity

Having fully characterized **RuSPDTC** and its aquation process, the biological properties of this complex were investigated within the TNBC MDA-MB-231 cell line.[59] The efficacy of **RuSPDTC** as both an MCU inhibitor and a cytotoxic agent is contingent on its ability to enter cells. Because PDTC is a Cu^{2+} ionophore that can increase intracellular Cu levels, triggering redox-mediated Cu^{2+}-dependent cytotoxicity,[60–62] the cytotoxicity and cellular uptake of **RuSPDTC** were investigated both in the presence and absence of added Cu^{2+}. Upon incubation of MDA-MB-231 cells with different concentrations of **RuSPDTC** or the free ligand PDTC in the presence or absence of 10 μM $CuSO_4$ for 48 h, the cell viability was determined by the MTT assay. As summarized in Table 2 and Fig. 4, the free ligand PDTC is cytotoxic against MDA-MB-231 cells,

as indicated by an IC_{50} value of 10.8 μM. Notably, the cytotoxicity of PDTC increases significantly in the presence of 10 μM $CuSO_4$, as the IC_{50} value decreases to 0.13 μM. **RuSPDTC** is similarly cytotoxic against this cell line, and its cytotoxicity also exhibits a dependence on Cu^{2+}. Notably, in the presence of $CuSO_4$, the IC_{50} value of **RuSPDTC** is 0.07 μM, a factor of two more cytotoxic than PDTC. This greater cytotoxicity is consistent with the fact that **RuSPDTC** brings two equivalents of PDTC to these cells, resulting in double the efficacy of the free ligand. As observed in other cell lines, Ru265 is non-toxic against MDA-MB-231 cells. This result confirms that the cytotoxic activity of **RuSPDTC** originates from the axial ligands rather than the Ru265′ core.

The cellular uptake of **RuSPDTC** and Ru265 in the presence and absence of 10 μM $CuSO_4$ was next studied. MDA-MB-231 cells were incubated with 50 μM of these compounds for 2 h prior to determining Ru and Cu concentrations with graphite furnace atomic absorption spectroscopy (GFAAS). The protein-normalized results are shown in Table 2 and Fig. S9 (SI). The intracellular Ru concentrations indicate that **RuSPDTC** is taken up by cells more effectively than Ru265, presumably due to the increased lipophilicity conferred by the organic PDTC ligands. With respect to intracellular Cu levels, both 100 μM PDTC and 50 μM **RuSPDTC** increase Cu uptake compared to Ru265. This result is consistent with the known Cu^{2+} ionophore properties of the PDTC.[63] The facilitated Cu uptake by **RuSPDTC** and PDTC is consistent with the observed cytotoxic properties of these compounds, as elevated intracellular Cu leads to ROS production and proteasome inhibition.[64,65] It is noteworthy that the Cu uptake in cells treated with **RuSPDTC** is greater than that induced by two equivalents of PDTC. This result suggests that the Ru core of **RuSPDTC** acts as a chaperone for PDTC, releasing optimal levels of this ligand either intracellularly or extracellularly to maximize its Cu^{2+} ionophore properties.

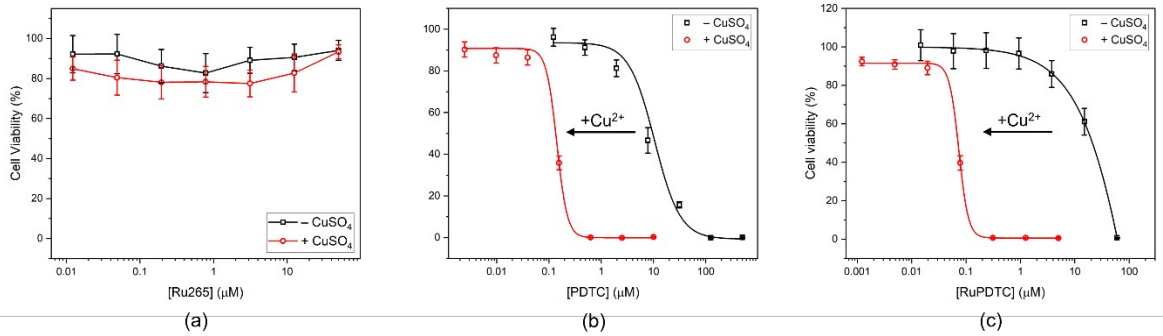

Fig. 4 Representative dose-response curves between cell viability and compound concentration of (a) Ru265, (b) PDTC and (c) **RuSPDTC** in MDA-MB-231 cells. Black traces represent test compounds alone and red traces represent test compounds + 10 μM $CuSO_4$. Data are presented as mean ± SD, n = 6.

Table 2 Biological properties of Ru265, PDTC and **RuSPDTC**

	Ru265		PDTC		**RuSPDTC**	
	– Cu^{2+}	+ Cu^{2+}	– Cu^{2+}	+ Cu^{2+}	– Cu^{2+}	+ Cu^{2+}
Cytotoxicity IC_{50} (μM)[a]	> 50	> 50	10.8 ± 0.8	0.13 ± 0.02	19 ± 8	0.07 ± 0.01
Ru cellular uptake (pg Ru/μg protein)[b]	21 ± 7	20 ± 7	n/a	n/a	65 ± 20	60 ± 20

Cu cellular uptake (pg Cu/μg protein)[b,c]	n/a	15 ± 1	21 ± 3	110 ± 60	19 ± 4	400 ± 100

[a] 48 h incubation in MDA-MB-231 cells, 4000 cells/well.
[b] 2 h incubation in MDA-MB-231 cells with 50 μM Ru compounds or 100 μM PDTC ± 10 μM $CuSO_4$
[c] MDA-MB-231 cells treated with 10 μM $CuSO_4$ alone have Cu uptake of 14 ± 4 pg Cu/μg protein

MCU inhibition and anti-metastatic activity

After validation of the Cu^{2+}-dependent cytotoxicity of **RuSPDTC**, the ability of this compound and Ru265 to inhibit $_mCa^{2+}$ uptake in permeabilized MDA-MB-231 cells was investigated. Both Ru265 and **RuSPDTC** inhibit $_mCa^{2+}$ uptake with nanomolar IC_{50} values, reflecting their potency as MCU inhibitors (Table 3 and Fig. S10, SI). Comparing the IC_{50} values of these compounds, however, it is somewhat surprising that **RuSPDTC** exhibits similar inhibitory activity on MCU compared to Ru265. In prior studies, we found that axial ligand functionalization led to a decrease in potency that could be recovered after these ligands underwent aquation and released Ru265′.[26,30,27–29] To investigate this phenomenon further, we carried out molecular docking studies to probe the interaction of **RuSPDTC** with the human MCU. These docking studies reveal that **RuSPDTC** cannot reside vertically in the MCU pore opening as has previously been proposed for Ru265′, which interacts via hydrogen bonding with ASP261 and GLU264 in the DIME region.[25] By contrast, **RuSPDTC** sits horizontally over the pore opening, forming hydrogen bonds only with ASP261 (Fig. S11, SI). This interaction is similar to that proposed for cobalt amine complexes that also exhibit MCU inhibitory properties.[25] The JC-1 assay in intact MDA-MB-231 cells was carried out to determine if **RuSPDTC** compromises mitochondrial integrity. After treating these cells with 10 μM of this compound for 1 h, no changes in the mitochondrial membrane potential (Ψ_m) were detected (Fig. S12, SI). These results suggest that mitochondrial depolarization is not the mechanism by which this compound inhibits $_mCa^{2+}$ uptake. Free PDTC ligand was also evaluated for its effect on $_mCa^{2+}$ uptake, but this compound failed to show any inhibitory properties at concentrations up to 1000 nM (Table 3 and Fig. S10, SI). Thus, the ability to inhibit $_mCa^{2+}$ uptake arises solely from the presence of the Ru core structure in **RuSPDTC**.

Given the role that the MCU plays in tumor metastasis, we next investigated the ability of **RuSPDTC** to slow down cell migration using the scratch assay. In this assay, a confluent monolayer of MDA-MB-231 cells wounded with a scratch to create a region free of cells was incubated with FBS-deficient cell culture medium supplemented with either Ru265, **RuSPDTC**, or PDTC. The closure of this gap in cells was monitored over the course of 24 h, a time period during which these test compounds are not cytotoxic (Fig. 5c). After this time period, untreated cells were able to nearly entirely fill the previously empty region of the dish. For cells treated with PDTC, however, the wound area remained larger than that of the control, indicative of the anti-migratory effects of this compound (Fig. 5). These results are consistent with prior studies that demonstrated PDTC to inhibit the NF-κB pathway and block the expression of matrix metalloproteinase, which breaks down the extracellular matrix to facilitate cell migration and metastasis.[66–68] Cells treated with Ru265, likewise exhibited a decrease in migration and wound closure (Fig. 5). This result is consistent with earlier studies that showed that the impure MCU inhibitor ruthenium red could also exhibit anti-metastatic and anti-migratory properties. Lastly, cells treated with **RuSPDTC** had the

smallest migratory activity, as revealed by a significantly larger wound remaining after 24 h. As a dual-function compound, it is likely that the improved anti-migratory activity of **RuSPDTC** is a result of complementary inhibitory activities of Ru265 and PDTC, which act via different pathways.

Table 3 IC_{50} values of Ru265, **RuSPDTC**, and PDTC for $_{m}Ca^{2+}$ uptake inhibition in permeabilized MDA-MB-231 cells (5×10^{6} cells/mL).

	IC_{50} (nM)[a]
Ru265	5 ± 3
RuSPDTC	4.2 ± 0.3
PDTC	>1000

[a] Data are reported as mean ± SD, n = 3

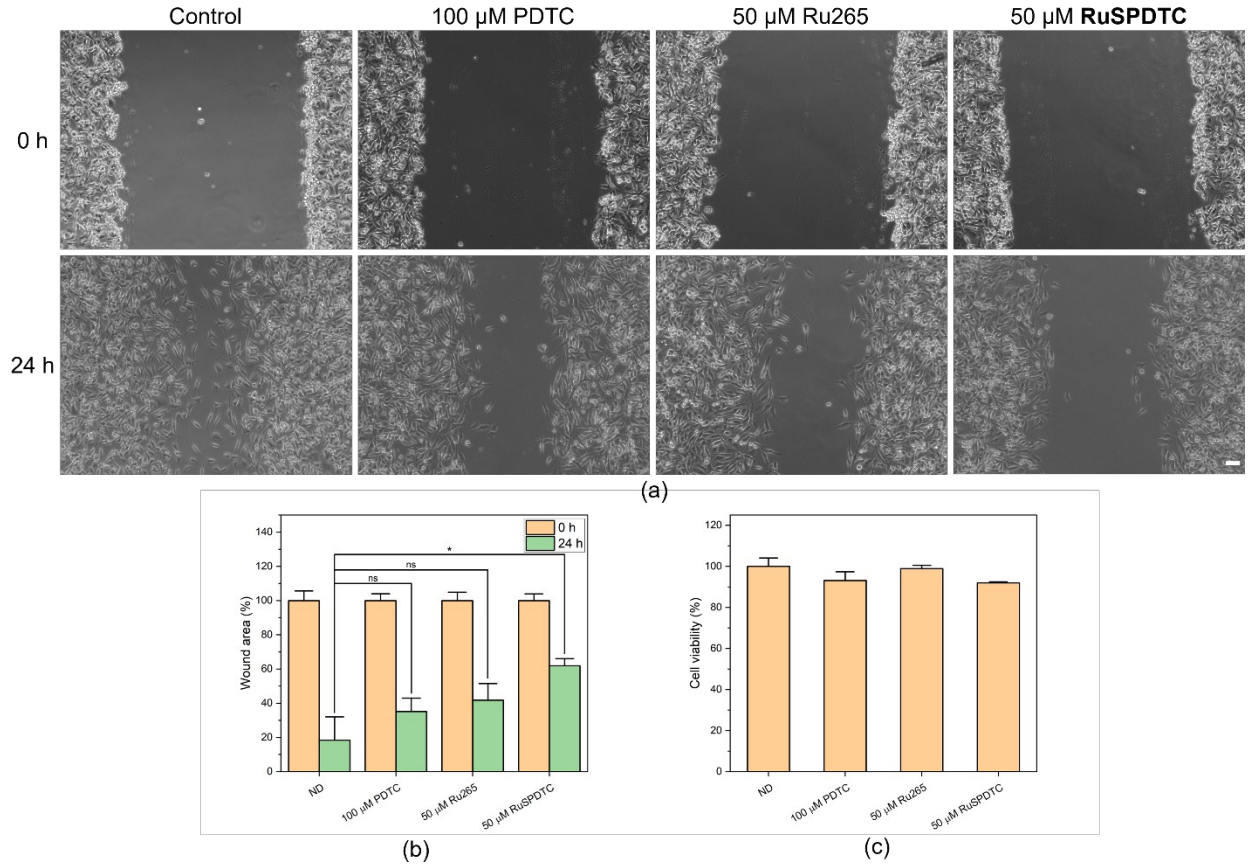

Fig. 5 Scratch assay on MDA-MB-231 cells. (a) Representative phase-contrast microscopy images of wound healing of MDA-MB-231 before and after 24 h of compound treatment (scale bar = 100 µm). (b) Quantification of wound area before and after 24 h of treatment using ImageJ. (c) Cell viability measurement after 24 h of treatment. Data are presented as mean ± SD, n = 3. Statistical significance measure with the Analysis of Variance (ANOVA) method. ns = not significant; * = $p < 0.05$.

Conclusion

In this work, we have developed a dual-function anticancer agent **RuSPDTC** by attaching the anticancer-active PDTC ligand to the MCU inhibitor Ru265. Notably, this compound is the first

Ru265 analogue featuring a S-based ligand at the axial position. Furthermore, to the best of our knowledge, this is also the second crystal structure reported of a Ru complex with a monodentate dithiocarbamate ligand. These findings significantly expand the coordination chemistry of Ru265-based compounds and allow more possibilities for prodrug development. Most importantly, **RuSPDTC** exhibits novel biological properties. The combination of the cytotoxic PDTC ligand with the MCU-inhibiting Ru265′ core to reduce cancer cell metastasis. Our results have shown that the prodrug can be activated through aquation under physiological conditions to release bioactive Ru265′ and PDTC, both of which retained their designated biological activities. In vitro studies have revealed that **RuSPDTC** exhibits potent Cu-dependent cytotoxicity arising from PDTC ligand with a sub-micromolar IC_{50} value, and simultaneously, shows potent MCU inhibition, which leads to decreased cell mobility. By combining anti-metastatic and cytotoxic functions within a single scaffold, **RuSPDTC** offers a promising systematic treatment strategy for invasive cancers like TNBC. Overall, this work establishes a proof-of-concept study for the development of dual-function Ru265-based therapeutic agents. Utilizing the versatility of the Ru265 scaffold, future investigations can be focused on the screening and incorporation of alternative bioactive ligands that can induce synergistic therapeutic effects and optimize pharmacological properties of Ru265-based prodrugs.

Data availability

Experimental procedure and the data supporting this article have been included as part of the ESI. Crystallographic data for **RuSPDTC** has been deposited at the CCDC under 2561884.

Conflicts of interest

The authors declare no conflict of interest.

Acknowledgement

This work was supported by the University of California, Santa Barbara (UCSB) and the U.S. National Science Foundation (NSF) (award number CHE-2414429). This work made use of the UCSB NMR facility, which is supported by the NSF under award number MRI-1920299. This work also made use of the UCSB Mass Spectrometry Facility, which was supported by the Office of Navy Research under award number N00014-23-2197. We are grateful to Dr. Guang Wu for assistance with single crystal XRD data collection and refinement. We thank Prof. Claudia Fischbach-Teschl at Cornell University for generously providing the MDA-MB-231 cell line used in this study.

Reference

1 R. L. Siegel, T. B. Kratzer, N. S. Wagle, H. Sung, A. Jemal, Cancer statistics, 2026, *CA. Cancer J. Clin.*, 2026, **76**, e70043.

2 E. Orrantia-Borunda, P. Anchondo-Nuñez, L. E. Acuña-Aguilar, F. O. Gómez-Valles, C. A. Ramírez-Valdespino, in *Breast Cancer*, ed. H. N. Mayrovitz, Exon Publications, Brisbane (AU), 2022, Subtypes of breast cancer.
3 O. J. Scully, B.-H. Bay, G. Yip, Y. Yu, Breast cancer metastasis, *Cancer Genomics Proteomics*, 2012, **9**, 311–320.
4 X. Xiong, L.-W. Zheng, Y. Ding, Y.-F. Chen, Y.-W. Cai, L.-P. Wang, L. Huang, C.-C. Liu, Z.-M. Shao, K.-D. Yu, Breast cancer: pathogenesis and treatments, *Signal Transduct. Target. Ther.*, 2025, **10**, 49.
5 F. Cardoso, S. Paluch-Shimon, E. Schumacher-Wulf, L. Matos, K. Gelmon, M. S. Aapro, J. Bajpai, C. H. Barrios, J. Bergh, E. Bergsten-Nordström, L. Biganzoli, M. J. Cardoso, L. A. Carey, M. Chavez-MacGregor, R. Chidebe, J. Cortés, G. Curigliano, R. A. Dent, N. S. El Saghir, A. Eniu, L. Fallowfield, P. A. Francis, S. X. Franco Millan, J. Gilchrist, J. Gligorov, W. J. Gradishar, R. Haidinger, N. Harbeck, X. Hu, R. Kaur, B. Kiely, S.-B. Kim, S. Koppikar, M. J. J. Kuper-Hommel, F. E. Lecouvet, G. Mason, S. A. Mertz, V. Mueller, C. Myerson, S. Neciosup, B. V. Offersen, S. Ohno, O. Pagani, A. H. Partridge, F. Penault-Llorca, A. Prat, H. S. Rugo, E. Senkus, G. W. Sledge, S. M. Swain, C. Thomssen, D. A. Vorobiof, P. Vuylsteke, T. Wiseman, B. Xu, A. Costa, L. Norton, E. P. Winer, 6th and 7th International consensus guidelines for the management of advanced breast cancer (ABC guidelines 6 and 7), *The Breast*, 2024, **76**, 103756.
6 G. Bianchini, C. De Angelis, L. Licata, L. Gianni, Treatment landscape of triple-negative breast cancer — expanded options, evolving needs, *Nat. Rev. Clin. Oncol.*, 2022, **19**, 91–113.
7 X. Jin, P. Mu, Targeting breast cancer metastasis, *Breast Cancer Basic Clin. Res.*, 2015, **9(S1)**, 23–34.
8 B. L. Eckhardt, P. A. Francis, B. S. Parker, R. L. Anderson, Strategies for the discovery and development of therapies for metastatic breast cancer, *Nat. Rev. Drug Discov.*, 2012, **11**, 479–497.
9 D. De Stefani, A. Raffaello, E. Teardo, I. Szabò, R. Rizzuto, A forty-kilodalton protein of the inner membrane is the mitochondrial calcium uniporter, *Nature*, 2011, **476**, 336–340.
10 J. M. Baughman, F. Perocchi, H. S. Girgis, M. Plovanich, C. A. Belcher-Timme, Y. Sancak, X. R. Bao, L. Strittmatter, O. Goldberger, R. L. Bogorad, V. Koteliansky, V. K. Mootha, Integrative genomics identifies MCU as an essential component of the mitochondrial calcium uniporter, *Nature*, 2011, **476**, 341–345.
11 T.-I. Peng, M.-J. Jou, Oxidative stress caused by mitochondrial calcium overload, *Ann. N. Y. Acad. Sci.*, 2010, **1201**, 183–188.
12 J. J. Lemasters, T. P. Theruvath, Z. Zhong, A.-L. Nieminen, Mitochondrial calcium and the permeability transition in cell death, *Biochim. Biophys. Acta BBA - Bioenerg.*, 2009, **1787**, 1395–1401.
13 A. Vultur, C. S. Gibhardt, H. Stanisz, I. Bogeski, The role of the mitochondrial calcium uniporter (MCU) complex in cancer, *Pflüg. Arch. - Eur. J. Physiol.*, 2018, **470**, 1149–1163.
14 E. Fernandez Garcia, U. Paudel, M. C. Noji, C. E. Bowman, A. K. Rustgi, J. R. Pitarresi, K. E. Wellen, Z. Arany, J. S. Weissenrieder, J. K. Foskett, The mitochondrial Ca^{2+} channel MCU is critical for tumor growth by supporting cell cycle progression and proliferation, *Front. Cell Dev. Biol.*, 2023, **11**.
15 C. Cui, J. Yang, L. Fu, M. Wang, X. Wang, Progress in understanding mitochondrial calcium uniporter complex-mediated calcium signalling: a potential target for cancer treatment, *Br. J. Pharmacol.*, 2019, **176**, 1190–1205.
16 S. Tang, X. Wang, Q. Shen, X. Yang, C. Yu, C. Cai, G. Cai, X. Meng, F. Zou, Mitochondrial Ca^{2+} uniporter is critical for store-operated Ca^{2+} entry-dependent breast cancer cell migration, *Biochem. Biophys. Res. Commun.*, 2015, **458**, 186–193.

17 A. Tosatto, R. Sommaggio, C. Kummerow, R. B. Bentham, T. S. Blacker, T. Berecz, M. R. Duchen, A. Rosato, I. Bogeski, G. Szabadkai, R. Rizzuto, C. Mammucari, The mitochondrial calcium uniporter regulates breast cancer progression via HIF-1α, *EMBO Mol. Med.*, 2016, **8**, 569–585.

18 T. Ren, H. Zhang, J. Wang, J. Zhu, M. Jin, Y. Wu, X. Guo, L. Ji, Q. Huang, H. Zhang, H. Yang, J. Xing, MCU-dependent mitochondrial Ca^{2+} inhibits NAD^{+}/SIRT3/SOD2 pathway to promote ROS production and metastasis of HCC cells, *Oncogene*, 2017, **36**, 5897–5909.

19 X. Wang, Y. Li, Z. Li, S. Lin, H. Wang, J. Sun, C. Lan, L. Wu, D. Sun, C. Huang, P. K. Singh, N. Hempel, M. Trebak, G. M. DeNicola, J. Hao, S. Yang, Mitochondrial calcium uniporter drives metastasis and confers a targetable cystine dependency in pancreatic cancer, *Cancer Res.*, 2022, **82**, 2254–2268.

20 Y. Liu, M. Jin, Y. Wang, J. Zhu, R. Tan, J. Zhao, X. Ji, C. Jin, Y. Jia, T. Ren, J. Xing, MCU-induced mitochondrial calcium uptake promotes mitochondrial biogenesis and colorectal cancer growth, *Signal Transduct. Target. Ther.*, 2020, **5**, 59.

21 H.-Y. Lin, P.-Y. Chu, Mitochondrial calcium uniporter as biomarker and therapeutic target for breast cancer: prognostication, immune microenvironment, epigenetic regulation and precision medicine, *J. Adv. Res.*, 2025, **70**, 445–461.

22 J. J. Woods, J. Lovett, B. Lai, H. H. Harris, J. J. Wilson, Redox stability controls the cellular uptake and activity of ruthenium-based inhibitors of the mitochondrial calcium uniporter (MCU), *Angew. Chem. Int. Ed.*, 2020, **59**, 6482–6491.

23 A. T. Baker, J. H. Lovett, H. Zou, J. J. Wilson, H. H. Harris, EXAFS analysis of Ru265 and Ru360 in human blood, *Inorg. Chem.*, 2026, **65**, 3606–3616.

24 J. J. Woods, N. Nemani, S. Shanmughapriya, A. Kumar, M. Zhang, S. R. Nathan, M. Thomas, E. Carvalho, K. Ramachandran, S. Srikantan, P. B. Stathopulos, J. J. Wilson, M. Madesh, A selective and cell-permeable mitochondrial calcium uniporter (MCU) inhibitor preserves mitochondrial bioenergetics after hypoxia/reoxygenation injury, *ACS Cent. Sci.*, 2019, **5**, 153–166.

25 J. J. Woods, M. X. Rodriguez, C.-W. Tsai, M.-F. Tsai, J. J. Wilson, Cobalt amine complexes and Ru265 interact with the DIME region of the mitochondrial calcium uniporter, *Chem. Commun.*, 2021, **57**, 6161–6164.

26 N. P. Bigham, Z. Huang, J. Spivey, J. J. Woods, S. N. MacMillan, J. J. Wilson, Carboxylate-capped analogues of Ru265 are MCU inhibitor prodrugs, *Inorg. Chem.*, 2022, **61**, 17299–17312.

27 Z. Huang, J. A. Spivey, S. N. MacMillan, J. J. Wilson, A ferrocene-containing analogue of the MCU inhibitor Ru265 with increased cell permeability, *Inorg. Chem. Front.*, 2023, **10**, 591–599.

28 N. P. Bigham, R. J. Novorolsky, K. R. Davis, H. Zou, S. N. MacMillan, M. J. Stevenson, G. S. Robertson, J. J. Wilson, Supramolecular delivery of dinuclear ruthenium and osmium MCU inhibitors, *Inorg. Chem. Front.*, 2024, **11**, 5064–5079.

29 H. Zou, S. N. MacMillan, J. J. Wilson, Employing phosphonate and phosphinate ligands for prodrug development of the mitochondrial calcium uniporter inhibitor Ru265, *J. Inorg. Biochem.*, 2026, **275**, 113145.

30 Z. Huang, S. N. MacMillan, J. J. Wilson, A fluorogenic inhibitor of the mitochondrial calcium uniporter, *Angew. Chem. Int. Ed.*, 2023, **62**, e202214920.

31 R. Schreck, B. Meier, D. N. Männel, W. Dröge, P. A. Baeuerle, Dithiocarbamates as potent inhibitors of nuclear factor kappa B activation in intact cells., *J. Exp. Med.*, 1992, **175**, 1181–1194.

32 S. F. Liu, X. Ye, A. B. Malik, Inhibition of NF-κB activation by pyrrolidine dithiocarbamate prevents in vivo expression of proinflammatory genes, *Circulation*, 1999, **100**, 1330–1337.

33 G. Tu, Z. Yao, Pyrrolidine dithiocarbamate inhibits NF-κB activation and enhances TNF-induced apoptosis in human breast cancer cells, *Chin. J. Cancer Res.*, 2004, **16**, 99–104.

34 D. Moellering, J. McAndrew, H. Jo, V. M. Darley-Usmar, Effects of pyrrolidine dithiocarbamate on endothelial cells: protection against oxidative stress, *Free Radic. Biol. Med.*, 1999, **26**, 1138–1145.

35 X. Shi, S. S. Leonard, S. Wang, M. Ding, Antioxidant properties of pyrrolidine dithiocarbamate and its protection against Cr(VI)-induced DNA strand breakage, *Ann. Clin. Lab. Sci.*, 2000, **30**, 209–216.
36 C. S. I. Nobel, M. Kimland, B. Lind, S. Orrenius, A. F. G. Slater, Dithiocarbamates induce apoptosis in thymocytes by raising the intracellular level of redox-active copper, *J. Biol. Chem.*, 1995, **270**, 26202–26208.
37 W. Erl, C. Weber, G. K. Hansson, Pyrrolidine dithiocarbamate-induced apoptosis depends on cell type, density, and the presence of Cu^{2+} and Zn^{2+}, *Am. J. Physiol.-Cell Physiol.*, 2000, **278**, C1116–C1125.
38 Y.-W. Chen, K.-L. Chen, C.-H. Chen, H.-C. Wu, C.-C. Su, C.-C. Wu, T.-D. Way, D.-Z. Hung, C.-C. Yen, Y.-T. Yang, T.-H. Lu, Pyrrolidine dithiocarbamate (PDTC)/Cu complex induces lung epithelial cell apoptosis through mitochondria and ER-stress pathways, *Toxicol. Lett.*, 2010, **199**, 333–340.
39 V. Milacic, D. Chen, L. Giovagnini, A. Diez, D. Fregona, Q. P. Dou, Pyrrolidine dithiocarbamate-zinc(II) and -copper(II) complexes induce apoptosis in tumor cells by inhibiting the proteasomal activity, *Toxicol. Appl. Pharmacol.*, 2008, **231**, 24–33.
40 L. Giovagnini, E. Mancinetti, L. Ronconi, S. Sitran, L. Marchiò, I. Castagliuolo, P. Brun, A. Trevisan, D. Fregona, Preliminary chemico-biological studies on Ru(III) compounds with *S*-methyl pyrrolidine/dimethyl dithiocarbamate, *J. Inorg. Biochem.*, 2009, **103**, 774–782.
41 E. M. Nagy, C. Nardon, L. Giovagnini, L. Marchiò, A. Trevisan, D. Fregona, Promising anticancer mono- and dinuclear ruthenium(III) dithiocarbamato complexes: systematic solution studies, *Dalton Trans.*, 2011, **40**, 11885–11895.
42 E. M. Nagy, A. Pettenuzzo, G. Boscutti, L. Marchiò, L. Dalla Via, D. Fregona, Ruthenium(II/III)-based compounds with encouraging antiproliferative activity against non-small-cell lung cancer, *Chem. – Eur. J.*, 2012, **18**, 14464–14472.
43 S. Scintilla, L. Brustolin, A. Gambalunga, F. Chiara, A. Trevisan, C. Nardon, D. Fregona, Ru(III) anticancer agents with aromatic and non-aromatic dithiocarbamates as ligands: loading into nanocarriers and preliminary biological studies, *J. Inorg. Biochem.*, 2016, **165**, 159–169.
44 A. W. DeMartino, M. Lima Souza, P. C. Ford, Uncaging carbon disulfide. Delivery platforms for potential pharmacological applications: a mechanistic approach, *Chem. Sci.*, 2017, **8**, 7186–7196.
45 D. Pugh, G. Hogarth, Addressing misconceptions in dithiocarbamate chemistry, *Dalton Trans.*, 2025, **54**, 11464–11494.
46 J. J. Woods, J. A. Spivey, J. J. Wilson, A [^{1}H,^{15}N] heteronuclear single quantum coherence NMR study of the solution reactivity of the ruthenium-based mitochondrial calcium uniporter inhibitor Ru265, *Eur. J. Inorg. Chem.*, 2022, **2022**, e202100995.
47 Q. J. McCubbin, F. J. Stoddart, T. Welton, A. J. P. White, D. J. Williams, Dithiocarbamate-functionalized dendrimers as ligands for metal complexes, *Inorg. Chem.*, 1998, **37**, 3753–3758.
48 M. Z. Aldin, G. Zaragoza, L. Delaude, Synthesis of ruthenium–dithiocarbamate chelates bearing diphosphine ligands and their use as latent initiators for atom transfer radical additions, *J. Organomet. Chem.*, 2021, **950**, 121993.
49 C. Preti, G. Tosi, P. Zannini, Synthesis and characterization of ruthenium dithiocarbamate complexes, *J. Inorg. Nucl. Chem.*, 1979, **41**, 485–488.
50 H. L. M. Van Gaal, J. W. Diesveld, F. W. Pijpers, J. G. M. Van Der Linden, Carbon-13 NMR spectra of dithiocarbamates. chemical shifts, carbon-nitrogen stretching vibration frequencies and π-bonding in the NCS_2 fragment, *Inorg. Chem.*, 1979, **18**, 3251–3260.
51 M. Altaf, M. Monim-ul-Mehboob, A. A. A. Seliman, A. A. Isab, V. Dhuna, G. Bhatia, K. Dhuna, Synthesis, X-ray structures, spectroscopic analysis and anticancer activity of novel gold(I) carbene complexes, *J. Organomet. Chem.*, 2014, **765**, 68–79.

52 M. Altaf, M. Monim-ul-Mehboob, A. A. Isab, V. Dhuna, G. Bhatia, K. Dhuna, S. Altuwaijri, The synthesis, spectroscopic characterization and anticancer activity of new mono and binuclear phosphanegold(I) dithiocarbamate complexes, *New J. Chem.*, 2014, **39**, 377–385.

53 F. Bonati, R. Ugo, Organotin(IV) N,N-disubstituted dithiocarbamates, *J. Organomet. Chem.*, 1967, **10**, 257–268.

54 D. H. Johnston, D. F. Shriver, Vibrational study of the trifluoromethanesulfonate anion: unambiguous assignment of the asymmetric stretching modes, *Inorg. Chem.*, 1993, **32**, 1045–1047.

55 A. Domenicano, A. Vaciago, L. Zambonelli, P. L. Loader, L. M. Venanzi, The structure of nitrosylruthenium tris-(*NN*-diethyldithiocarbamate): a complex with a monodentate dithiocarbamate group, *Chem. Commun. Lond.*, 1966, 476–477.

56 J. V. Dubrawski, R. D. Feltham, Bis(dithiocarbamato)-nitrosyl complexes of ruthenium, *Inorg. Chem.*, 1980, **19**, 355–363.

57 B. R. Cameron, M. C. Darkes, I. R. Baird, R. T. Skerlj, Z. L. Santucci, S. P. Fricker, Ruthenium(III) triazacyclononane dithiocarbamate, pyridinecarboxylate, or aminocarboxylate complexes as scavengers of nitric oxide, *Inorg. Chem.*, 2003, **42**, 4102–4108.

58 P. W. G. Newman, C. L. Raston, A. H. White, Crystal structures of bis(pyrrolidonecarbodithioato)-nickel(II) and -copper(II), *J. Chem. Soc. Dalton Trans.*, 1973, 1332–1335.

59 K. J. Chavez, S. V. Garimella, S. Lipkowitz, Triple negative breast cancer cell lines: one tool in the search for better treatment of triple negative breast cancer, *Breast Dis.*, 2010, **32**, 35–48.

60 K. G. Daniel, D. Chen, S. Orlu, Q. C. Cui, F. R. Miller, Q. P. Dou, Clioquinol and pyrrolidine dithiocarbamate complex with copper to form proteasome inhibitors and apoptosis inducers in human breast cancer cells, *Breast Cancer Res.*, 2005, **7**, R897.

61 M. J. Burkitt, H. S. Bishop, L. Milne, S. Y. Tsang, G. J. Provan, C. S. I. Nobel, S. Orrenius, A. F. G. Slater, Dithiocarbamate toxicity toward thymocytes involves their copper-catalyzed conversion to thiuram disulfides, which oxidize glutathione in a redox cycle without the release of reactive oxygen species, *Arch. Biochem. Biophys.*, 1998, **353**, 73–84.

62 C. S. I. Nobel, M. Kimland, B. Lind, S. Orrenius, A. F. G. Slater, Dithiocarbamates induce apoptosis in thymocytes by raising the intracellular level of redox-active copper, *J. Biol. Chem.*, 1995, **270**, 26202–26208.

63 B.-E. Kim, T. Nevitt, D. J. Thiele, Mechanisms for copper acquisition, distribution and regulation, *Nat. Chem. Biol.*, 2008, **4**, 176–185.

64 L. Chen, J. Min, F. Wang, Copper homeostasis and cuproptosis in health and disease, *Signal Transduct. Target. Ther.*, 2022, **7**, 378.

65 L. M. Gaetke, C. K. Chow, Copper toxicity, oxidative stress, and antioxidant nutrients, *Toxicology*, 2003, **189**, 147–163.

66 J. Zhang, Z. Xu, C. Zhang, H. Dai, X. Ji, X. Wang, C. Li, Pyrrolidine dithiocarbamate inhibits nuclear factor-κB pathway activation, and regulates adhesion, migration, invasion and apoptosis of endometriotic stromal cells, *Mol. Hum. Reprod.*, 2011, **17**, 175–181.

67 R. Tang, C. Mao, C. Hu, W. Liu, J. Bai, Y. Wang, L. Yang, H. Qi, Exosome membrane-biomimetic nanomedicine targets the pre-metastatic niche *via* NF-κB inhibition to suppress breast cancer lung metastasis, *Mater. Today Bio*, 2026, **37**, 102856.

68 M. A. Huber, N. Azoitei, B. Baumann, S. Grünert, A. Sommer, H. Pehamberger, N. Kraut, H. Beug, T. Wirth, NF-κB is essential for epithelial-mesenchymal transition and metastasis in a model of breast cancer progression, *J. Clin. Invest.*, 2004, **114**, 569–581.